

3. Process Models

The set of models used in this study applied to EAF process emphasizes the decarburization and reaction of carbonaceous materials with iron oxide in slag phase. Mass balance for relevant species in solution in iron melt, changes in the slag and gas composition are also included as well the estimate for overall melting rates for scrap blends and pig iron computed by inverse calculation. The summary of melting down and primary refining in EAF can be simplified as follows:

- The ferrous materials melt resulting in a liquid steel phase, called “Metal Phase”;
- Pure oxygen injected through lance injectors and/or available from the infiltration air react with ferrous materials and metal phase producing oxides, that float and dissolve in the “Slag Phase” or leave the control volume through the “Gas Phase”;
- The added slag formers dissolve in the slag phase;
- Portion of small particles present in the material blend is carried by the off-gas system, producing a “Dust Phase” in the bag-house outside of the control volume of the EAF;
- Carbonaceous materials react with oxygen and with iron oxide, producing gaseous carbon oxides, addressed to the “Gas Phase”;
- Carbonaceous materials may dissolve in the Fe metal phase under particular conditions;
- Natural gas or fossil fuel react with oxygen through burners, supplying carbon dioxide and water to the gas phase;

Figure 48 presents a diagram pointing out the main input and output materials.

Figure 49 suggests a typical mass balance applied to EAF process.

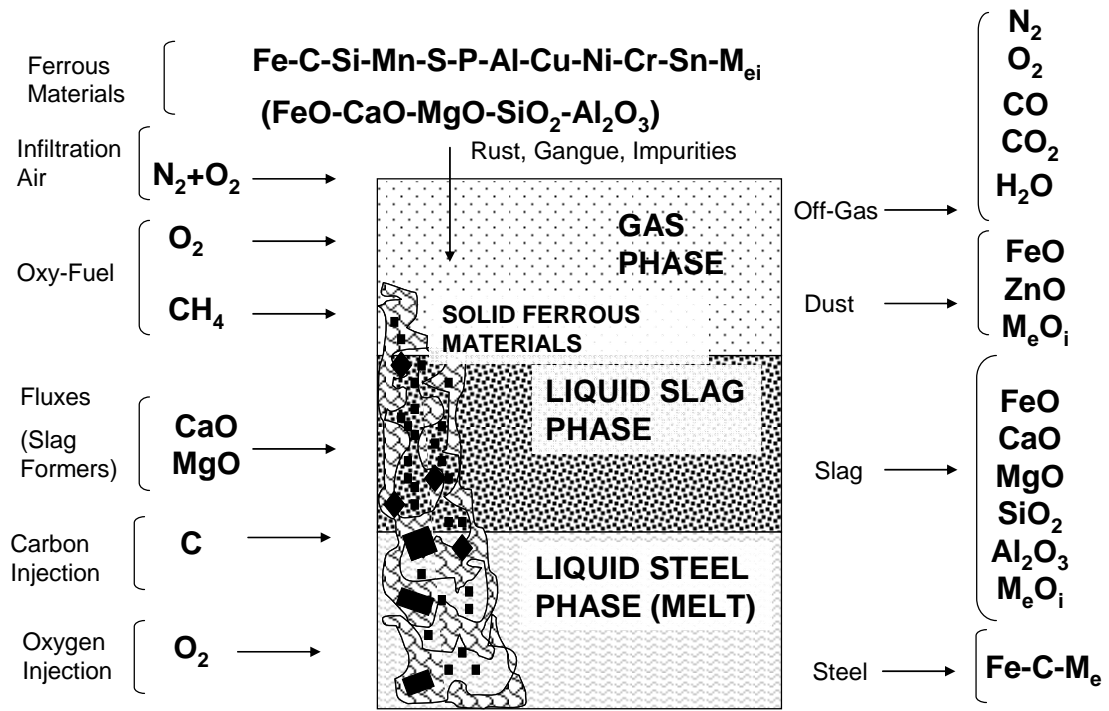


Figure 48 - Typical EAF Mass Flowchart

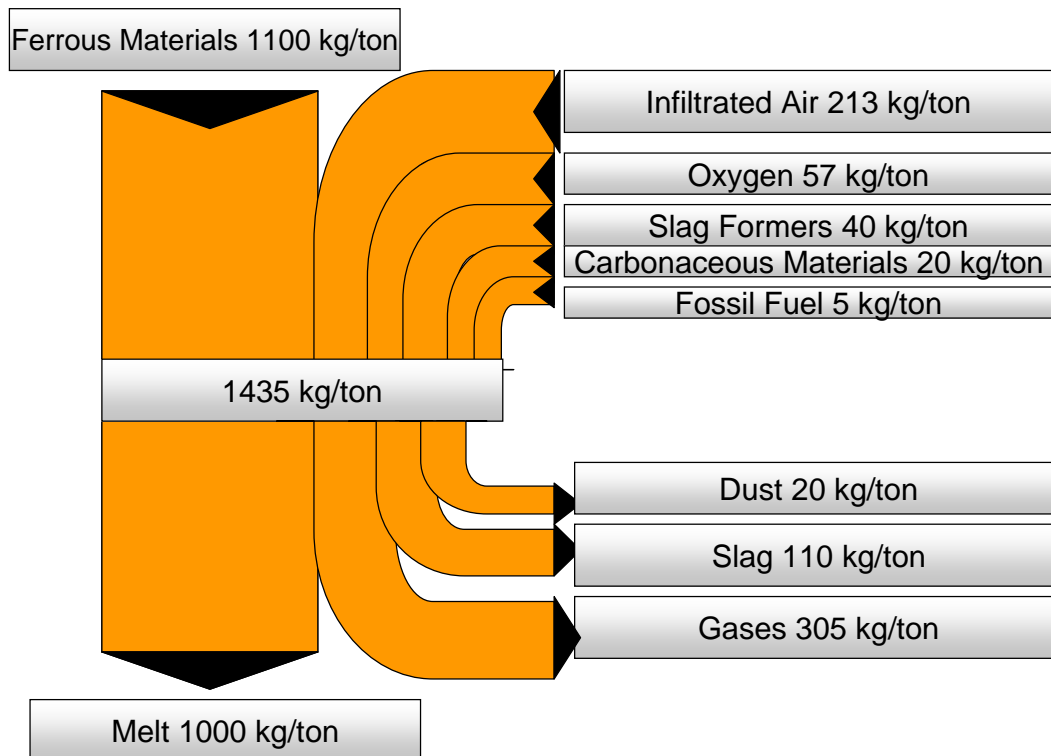


Figure 49 - Typical EAF Mass Balance

3.1. The main chemical reactions

The process model flow chart presented in Figure 50 as follows is a simplified description of mass balance proposed for the current algorithm. Even though the main focus is to estimate the evolution of carbon content in the metal phase, the slag amount and its chemical composition, other auxiliary models shall be used due to their interdependence such as Si, Mn and P oxidation models. The secondary models related to Al and Cr oxidation are add-on and accounted just for further process evaluation. The main chemical reactions considered for mass balance purposes are described below:

Note: the underlined symbols mean that the specie is dissolved in iron

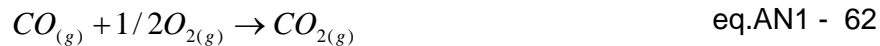
Carbon oxidation (carbonaceous material) – Partial Combustion



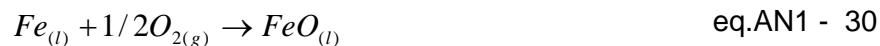
Carbon oxidation (carbonaceous material) – Complete Combustion



Carbon oxidation (Post combustion)



Iron oxidation



Iron oxide reduction



Manganese oxidation



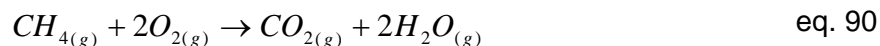
Silicon oxidation



Phosphorus oxidation



Natural gas (fossil fuel) oxidation



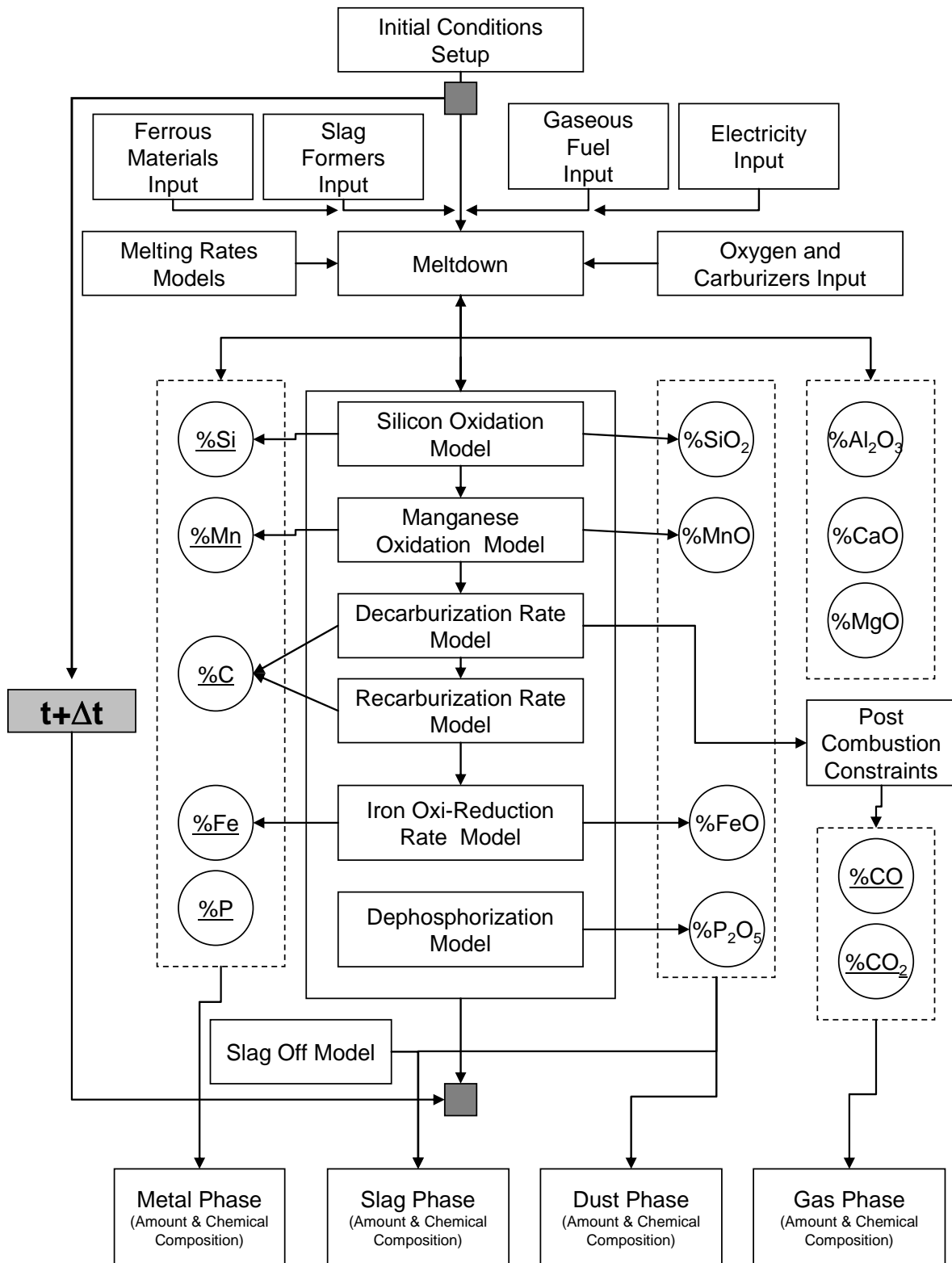


Figure 50 – EAF process flowchart

3.2. Control Volume

In respect of the control volume (CV) defined in the sketch presented in

Figure 51, the law of conservation of mass premise can be described as:

$$J_{In} - J_{Out} + J_{Acc} = 0 \quad \text{eq. 91}$$

where J_{In} is the rate of mass into CV; J_{Out} is the rate of mass outward CV and J_{Acc} is rate of accumulation of mass within CV. It is assumed that the accumulation rate is null after the EAF vessel has the ferrous charge complete. The density of all phases is considered constant.

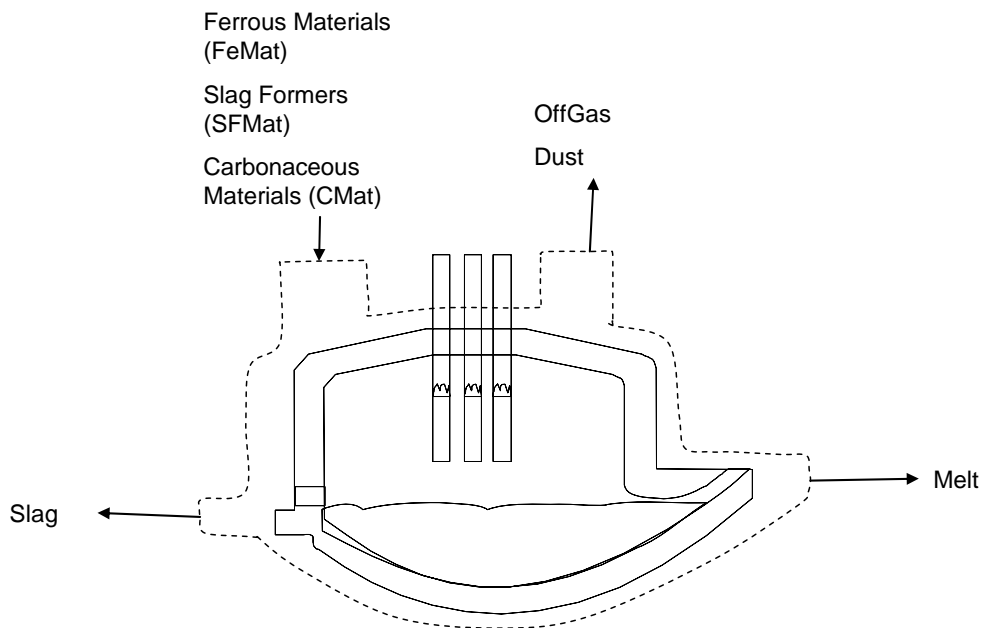


Figure 51 – EAF Control Volume

3.3. Ferrous Raw Materials Properties

In the proposed model, the ferrous materials consist usually of several scrap grades and pig iron. Pig iron is also called “Substitute” because they can replace scrap grades in the ferrous materials blend. Particularly in this chapter, the mass concentration is represented by $C_{Me_i}^{FeMat_i}$ [%]. The superscript “ $FeMat_i$ ” represents the Ferrous Materials grade: Scrap #1, Scrap #2,...,Scrap #n, Pig Iron, etc. The subscript “ Me_i ” identifies the components or species such as: C, Si, Mn, S, P and many others present in the bulk of ferrous materials (Cu, Ni, Cr, Sn, Al, Mo). For instance, the mass concentration is represented by $C_{Me_i}^{Scrap_i}$ and $C_{Me_i}^{PIron}$ [%], respectively.

Besides these simple elements, the presence of impurities entrapped on the materials surface is also considered. Their mass concentration notation is represented by $C_{Imp,MeO_i}^{FeMat_i}$, where the subscript “ MeO_i ” assumes the notation of oxides like CaO, MgO, SiO₂, Al₂O₃, P₂O₅. For example, $C_{Imp,SiO_2}^{Scrap_i}$ represents the mass concentration of SiO₂ in the impurities entrapped in the scrap. The mass concentration of iron oxide and volatiles (oil, grease, paintings) content usually present in the ferrous materials are represented by $C_{Rust}^{FeMat_i}$, $C_{Oil}^{FeMat_i}$ and $C_{Paint}^{FeMat_i}$.

Even though “Rust” is basically iron oxide, metallic iron particles are assumed to be found and some of them can be incorporated to the metal phase whenever it is charged. Hence a metallization index shall be defined as η_{Met}^{Rust} . This index influences the Fe-FeO mass balance.

$$\eta_{Met}^{Rust} = \frac{C_{Fe}^{Rust}}{C_{FeTotal}^{Rust}} \quad \text{eq. 92}$$

where,

$$C_{FeTotal}^{Rust} = C_{Fe}^{Rust} + C_{FeO}^{Rust} \cdot \frac{MW_{Fe}}{MW_{FeO}} \quad \text{eq. 93}$$

The concentration of iron oxides in the slag phase are often described as Fe_tO or FeO_t or FeO_x ,

$$\%Fe_tO \equiv \%FeO + 0.9 \cdot \%Fe_2O_3 \equiv \frac{MW_{FeO}}{MW_{Fe}} \cdot \%T.Fe \quad \text{eq. 94}$$

where $\%T.Fe$ is the measurement of total iron mass concentration.

For the sake of simplicity, the subscript “t” will be omitted in following sessions.

In contrast to the weight of volatile matter W^{Oil} and W^{Paint} which is all addressed to the gas phase, the Impurities and the rust charged in the EAF are partially carried to the bag house forming dust, and the remaining portion is assumed to be absorbed by the slag phase. Therefore, a dust partition coefficient $\eta_{Dust}^{FeMat_i}$ is defined as a function of area to volume ratio of each ferrous material grade (scrap grades and pig iron). They are input and will be described in section 3.7.4.

3.4. Slag Formers Properties

The usual slag formers are lime and dolomite. The symbols used for the mass concentration of components are $C_{Me_i}^{SFMat_i}$, and of oxide components is $C_{MeO_i}^{SFMat_i}$. The subscript “ MeO_i ” means a metal oxide (FeO, MnO, Al_2O_3 , CaO, and MgO) or non metal oxides (SiO_2 , P_2O_5). For example, oxide components for lime and dolomite are $C_{MeO_i}^{Lime}$ and $C_{MeO_i}^{Dolo}$, respectively. The slag formers can also contain moisture H_2O , not fully calcinated volume ($CaCO_3$ or $MgCO_3$) represented by CO_2 , and also some elements Me_i such as C and S are accounted by the model.

Refractory consumption $w^{Re\ fractory}$ regarding fettling materials is input, since it is a source of MgO in the slag $C_{MgO}^{Re\ frat}$.

3.5. Carbonaceous Materials Properties

The mass concentration notations of components in carbonaceous materials distinguish both charging processes: bucket charged and injected materials. Respectively, the mass concentration of oxides $C_{MeO_i}^{CMatCh_i}$ and $C_{MeO_i}^{CMatInj_i}$, and of other elements $C_{Me_i}^{CMatCh_i}$ and $C_{Me_i}^{CMatInj_i}$.

3.6. Initial Conditions Setup

Resident slag and hot heel properties vary among melt shop facilities, even between heats in the same EAF facility. In the most cases, there are no weight measurements for resident slag, and it influences the model accuracy in some extent. Every single heat has the hot heel and resident slag checked visually by experimented operators.

Initial conditions are setup such as: slag weight W_0^{Slag} , slag mass composition $C_{MeO_x,0}^{Slag}$ for CaO, MgO, SiO₂, FeO, Al₂O₃, P₂O₅, hot heel weight W_0^{Heel} , hot heel chemical composition $C_{Me,0}^{Melt}$ for C, Si, Mn, S and P.

3.7. Meltdown Model

Meltdown model handles the input data provided by ferrous raw materials, slag formers, carburizers, gases injection, electrical energy parameters, power on and power off times. Kinetic models managed by the Meltdown model compute simultaneously the chemistry and the amount of the molten metal W_t^{Melt} , slag W_t^{Slag} , dust W_t^{Dust} and gas at any time "t".

3.7.1. Processing Times

The Tap-to-Tap time t_{TTT} [min] is the total time consumed to process a heat.

$$t_{TTT} = t_{POn} + t_{POff} \quad \text{eq. 95}$$

where, t_{POn} is the power on time when the EAF is switched on) and t_{POff} is the power off time when the EAF is switched off for different reasons,

$$t_{POn} = \left(\frac{EE_{Melting}}{Pot_{Melting}} + \frac{EE_{Re\,fining}}{Pot_{Re\,fining}} \right) \cdot \frac{60}{1000} \quad \text{eq. 96}$$

where, EE_i is the electrical energy consumption [kWh/heat], Pot_i is the electrical power average in [MW], and 60 [min/h]

$$t_{POff} = t_{bkt} + t_{Tapping} + t_{Level} + t_{Prep} + t_T + t_{Others} \quad \text{eq. 97}$$

Respectively in sequence: charging buckets, tapping time, scrap leveling, bucket preparation, temperature measurement and other delays [min]

$$t_{bkt} = t_{Ch} \cdot n_{bkt} \quad \text{eq. 98}$$

where t_{Ch} is the time consumed per bucket and n_{bkt} is the number of buckets.

3.7.2. Melting and Dissolving Rates

The supervisory meltdown model manages the melting rates of ferrous materials as well the dissolution rates of their rust, impurities contents and slag formers. Dissolution rates for “Rust” and “Impurities” are defined as r_t^{Rust} and r_t^{Imp} in [kg/min], respectively. They can also be configured to be a function of time,

$$r_t^{Rust} = A0_{Rust}^{\#bkt} + A1_{Rust}^{\#bkt} \cdot t \quad \text{eq. 99}$$

$$r_t^{Imp} = A0_{Imp}^{\#bkt} + A1_{Imp}^{\#bkt} \cdot t \quad \text{eq. 100}$$

where the parameters $A0$ (kg/min) and $A1$ (kg/min²) are input. However, usually $A1$ is neglected and FeO melting rate is adopted [68, 72].

Dissolution rates for all slag formers materials such as lime and dolomite are defined as r_t^{SFMat} [kg/min], and can be configured to be a function of time,

$$r_t^{SFMat_i} = A0_{SlagFMat}^{\#bkt} + A1_{SlagFMat}^{\#bkt} \cdot t \quad \text{eq. 101}$$

where the parameters $A0$ (kg/min) and $A1$ (kg/min²) are input. As presumed for impurities and FeO, $A1$ can be neglected too. Dissolution rates measured under EAF operational conditions were adopted from literature [73, 74], $A0 = 150$ [kg/min]. The meltdown model manages the dissolving rates which maybe configured as a function of the charged bucket number “ $\#bkt$ ”. In addition, the yield for slag formers and carbon sources injected or charged may not be 100%. Hence yield coefficient are also defined as η_{SFMat_i} (η_{Lime} , η_{Dolo}), $\eta_{CMatInj}$, and η_{CMatCh} [%], respectively. For simplicity, refractory materials assume the same dissolving rate defined for slag formers. The total refractory mass to be dissolved is input according to average consumptions figures reported. In this study, the computed influence of refractory in the slag mass is very small.

Ferrous materials melting rate is represented by $r_t^{FeMat_i}$, and is related to the melting rates for the scrap mix and pig iron: $r_t^{Scrap_i}$ and r_t^{PIron} , respectively.

$$r_t^{Scrap} = A0_{Scrap}^{\#bkt} + A1_{Scrap}^{\#bkt} \cdot t \quad \text{eq. 102}$$

$$r_t^{PIron} = A0_{PIron}^{\#bkt} + A1_{PIron}^{\#bkt} \cdot t \quad \text{eq. 103}$$

In similar manner, melting rates of ferrous materials depend on processing time. Bucket charging results in a pile of ferrous materials submitted to a pre-heating step in the EAF vessel, because the hot heel and electric arc work like heat sources in the sill level. When meltdown is taking place in the lower layers, the remaining solid charge in the upper layers is presumed to melt faster than the previous layer, because the last layers are pre-heated through a longer period of time, and reaches the hot heel and/or the electric arc hotter. Other functions like polynomial were tested, but the linear model worked well too and made the algorithm calculation faster. Of course, the complexity of the transient heating in EAF is much more complicated, and some effort has been done in the last

decade, both by academic centers as well by technology companies. Nevertheless, just a few and incipient energy balance models are implemented as off-line industrial simulators. Available real time applications are far to be accurate mainly due to the unpredictable way the ferrous charge is fulfilling in the EAF vessel. The size and geometry of scrap grades are so diverse, making the prediction of the different layers interaction very difficult, and virtually not available for industrial application.

3.7.3. Charging (Solid Phase)

Batch charging can be setup to three buckets. The notations $W_{\#bkt}^{FeMat_i}$, $W_{\#bkt}^{SlagFMat_i}$, $W_{\#bkt}^{CMatCh_i}$ are the weight of ferrous, slag formers and carbonaceous materials charged per bucket charging event.

If charging is performed continuously in addition to bucket batch charge, feeding rates for different ferrous, slag formers and carbonaceous materials are data input: $Ch_t^{FeMatCCh_i}$, $Ch_t^{SFMatCCh_i}$, $Ch_t^{CMatCCh_i}$ in [kg/min], respectively. It is relevant for Consteel process or EAF based on DRI continuous charging through the roof. Equations eq. 104 to eq. 110 describe such formulation.

$$W_{t+\Delta t}^{FeMat} = \sum_{bkt\#=1}^{bkt\#=3} \sum_{i=1}^n W_{\#bkt}^{FeMat_i} + \sum_0^t Ch_t^{FeMatCCh_i} \cdot \Delta t \quad \text{eq. 104}$$

The weight charged of any component from ferrous materials at any time $t+\Delta t$

$$W_{Me_i, t+\Delta t}^{FeMat} = \left(\sum_{bkt\#=1}^{bkt\#=3} \sum_{i=1}^n W_{\#bkt}^{FeMat_i} + \sum_0^t Ch_t^{FeMatCCh_i} \cdot \Delta t \right) \cdot C_{Me_i}^{FeMat_i} \quad \text{eq. 105}$$

$$W_{MeO_i, t+\Delta t}^{FeMat} = W_{Im p, MeO_i, t+\Delta t}^{FeMat} + W_{Rust, MeO_i, t+\Delta t}^{FeMat} + W_{FeOBulk, t+\Delta t}^{FeMat} \quad \text{eq. 106}$$

$$W_{Im p, MeO_i, (t+\Delta t)}^{FeMat} = \left(\sum_{bkt\#=1}^{bkt\#=3} \sum_{i=1}^n W_{\#bkt}^{FeMat_i} + \sum_0^t Ch_t^{FeMatCCh_i} \cdot \Delta t \right) \cdot \left(C_{Im p, MeO_i}^{FeMat_i} \cdot C_{MeO_i}^{Im p} \right) \quad \text{eq. 107}$$

$$W_{Rust,MeO_i,(t+\Delta t)}^{FeMat} = \left(\sum_{bkt\#=1}^{bkt\#=3} \sum_{i=1}^n W_{\#bkt}^{FeMat_i} + \sum_0^t Ch_t^{FeMatCCh_i} \cdot \Delta t \right) \cdot (C_{Rust,MeO_i}^{FeMat_i} \cdot C_{MeO_i}^{Rust}) \quad \text{eq. 108}$$

$$W_{FeOBulk,(t+\Delta t)}^{FeMat} = \left(\sum_{bkt\#=1}^{bkt\#=3} \sum_{i=1}^n W_{\#bkt}^{FeMat_i} + \sum_0^t Ch_t^{FeMatCCh_i} \cdot \Delta t \right) \cdot (C_{FeOBulk}^{FeMat_i}) \quad \text{eq. 109}$$

3.7.4. Partition of Raw Materials

Oxides and simple components content in ferrous, slag formers and carbonaceous materials are distributed in different phases even before any chemical reaction. The oxygen injection, the negative pressure inside the EAF can remove part of the rust and impurities charged in ferrous materials. Moreover, depending on the size distribution of slag formers and carbonaceous materials, as well the technology applied for charging or injecting them into EAF control volume, portion of these raw materials could be carried out to the off gas system. Hence, it is necessary to estimate the mass partition of the Impurities, rust and simple components for the metal, slag, and dust phases immediately before the melting process has began.

3.7.4.1. Partition of Ferrous Materials

Figure 52 present the partition flow of rust, impurities and vaporized iron. Equation eq. 111 to eq. 119 compute the partitioned mass concentrations regarding any grade of ferrous materials.

The Impurities and Rust partition concentrations can be converted to mass at any time t by the eq. 110,

$$W_{Source,t}^{Destination} = (r_t^{FeMat_i} \cdot C_{Source,Me-MeO_i}^{FeMat_i} \Big|_{Destination}) \cdot \Delta t \quad \text{eq. 110}$$

where *Destination* = Metal, Slag or Dust; *Source* = Rust, Impurities;

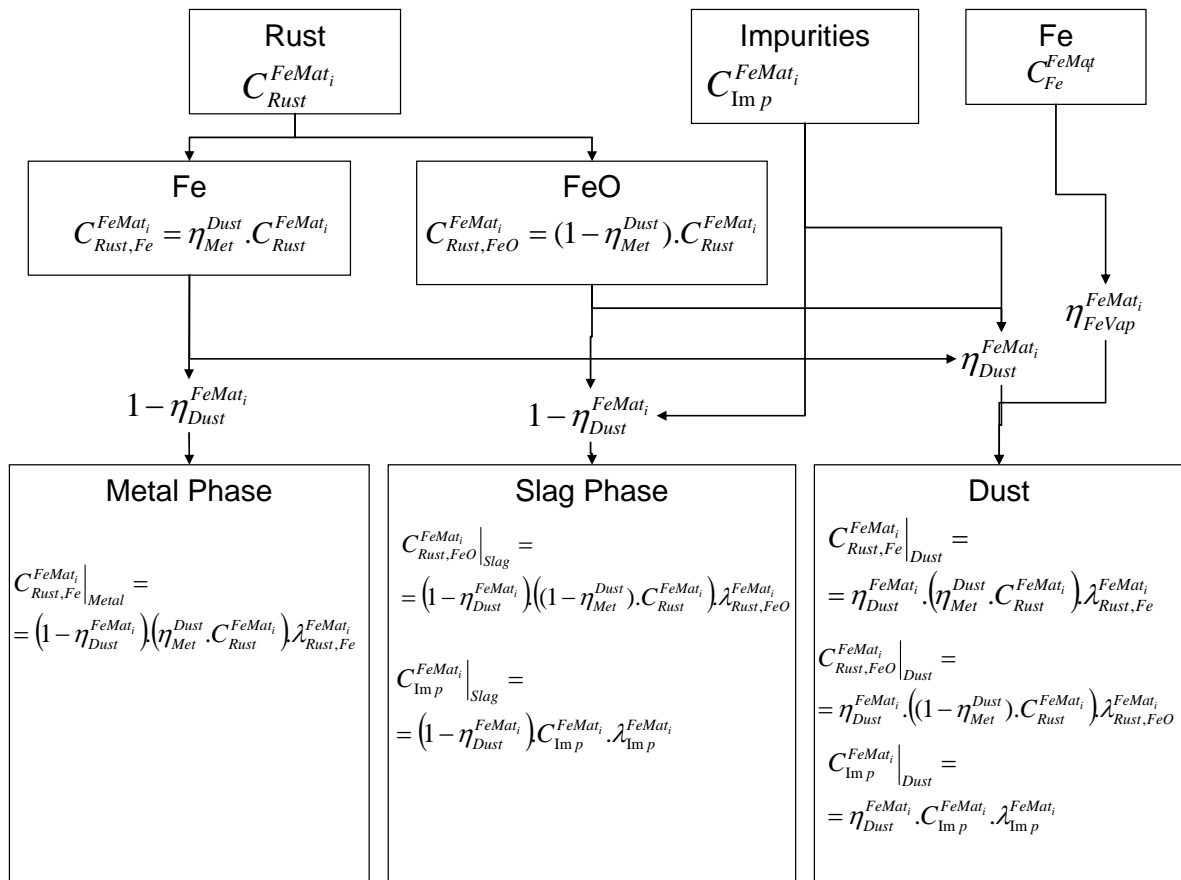


Figure 52 – Weight partition flow for Rust and Impurities content in the ferrous materials charge

To the metal phase

$$C_{Rust,Fe}^{Scrap} \Big|_{Metal} = (1 - \eta_{Dust}^{FeMat_i}) (\eta_{Met}^{Dust} \cdot C_{Rust}^{FeMat_i}) \lambda_{Rust,Fe}^{FeMat_i} \quad \text{eq. 111}$$

To the slag phase

$$C_{Rust,FeO}^{FeMat_i} \Big|_{Slag} = (1 - \eta_{Dust}^{FeMat_i}) ((1 - \eta_{Met}^{Dust}) \cdot C_{Rust}^{FeMat_i}) \lambda_{Rust,FeO}^{FeMat_i} \quad \text{eq. 112}$$

$$C_{Imp}^{FeMat_i} \Big|_{Slag} = (1 - \eta_{Dust}^{FeMat_i}) C_{Imp}^{FeMat_i} \lambda_{Imp}^{FeMat_i} \quad \text{eq. 113}$$

To the dust phase

$$C_{Rust,Fe}^{FeMat_i} \Big|_{Dust} = \eta_{Dust}^{FeMat_i} \cdot (\eta_{Met}^{Dust} \cdot C_{Rust}^{FeMat_i}) \cdot \lambda_{Rust,Fe}^{FeMat_i} \quad \text{eq. 114}$$

The iron carried to the dust will be oxidized to FeO at the bag house

$$C_{Rust,FeO}^{FeMat_i} \Big|_{Dust} = \eta_{Dust}^{FeMat_i} \cdot ((1 - \eta_{Met}^{Dust}) \cdot C_{Rust}^{FeMat_i}) \cdot \lambda_{Rust,FeO}^{FeMat_i} \quad \text{eq. 115}$$

$$C_{Imp}^{FeMat_i} \Big|_{Dust} = \eta_{Dust}^{FeMat_i} \cdot C_{Imp}^{FeMat_i} \cdot \lambda_{Imp}^{FeMat_i} \quad \text{eq. 116}$$

where, $\lambda_{i,j}^k$ is a mass balance factor where k = Scrap or Pig iron; i =Rust, Imp; j = (Fe, FeO and Imp)

$$\lambda_{Rust,FeO}^{FeMat_i} = \frac{C_{Rust,FeO}^{FeMat_i}}{C_{Rust,Fe}^{FeMat_i} + C_{Rust,FeO}^{FeMat_i} + C_{Imp}^{FeMat_i}} \quad \text{eq. 117}$$

$$\lambda_{Rust,Fe}^{FeMat_i} = \frac{C_{Rust,Fe}^{FeMat_i}}{C_{Rust,Fe}^{FeMat_i} + C_{Rust,FeO}^{FeMat_i} + C_{Imp}^{FeMat_i}} \quad \text{eq. 118}$$

$$\lambda_{Imp}^{FeMat_i} = \frac{C_{Imp}^{FeMat_i}}{C_{Rust,Fe}^{FeMat_i} + C_{Rust,FeO}^{FeMat_i} + C_{Imp}^{FeMat_i}} \quad \text{eq. 119}$$

3.7.4.2. Partition of Slag Formers Materials

Similar weight partition can be computed for slag former materials according to Figure 53, and for carbonaceous materials presented in Figure 54.

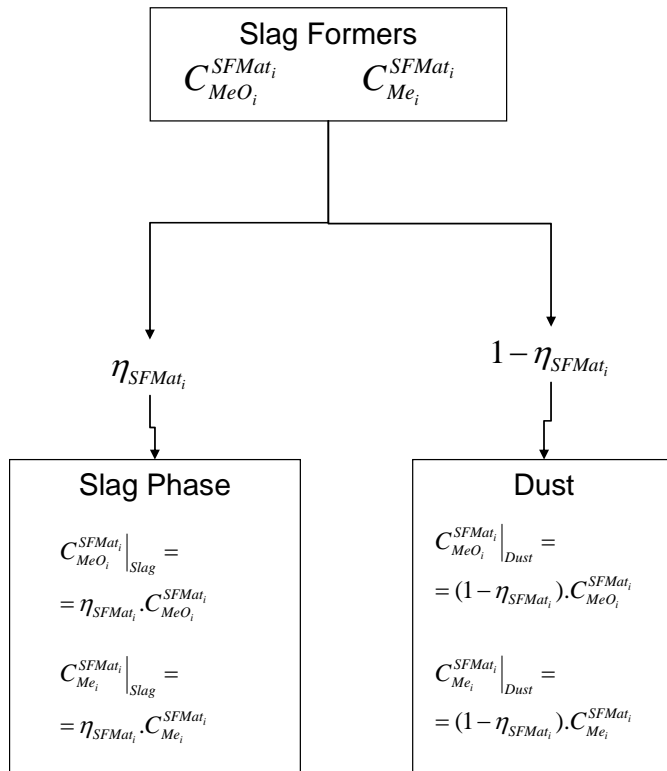


Figure 53 – Weight partition flow for elements and oxides content in the slag former materials

From slag formers materials

The eq. 120 to eq. 124 compute the partitioned mass concentrations regarding any grade of slag former materials.

$$W_{Source,t}^{Destination} = (r_t^{SFMat_i} \cdot C_{Source,Me-MeO_i}^{SFMat_i} \Big|_{Destination}) \cdot \Delta t \quad \text{eq. 120}$$

where *Destination* = Metal, Slag or Dust phases; *Source* = Rust, Impurities;

To the slag phase

$$C_{MeO_i}^{SFMat_i} \Big|_{Slag} = \eta_{SFMat_i} \cdot C_{MeO_i}^{SFMat_i} \quad \text{eq. 121}$$

$$C_{Me_i}^{SFMat_i} \Big|_{Slag} = \eta_{SFMat_i} \cdot C_{Me_i}^{SFMat_i} \quad \text{eq. 122}$$

To the dust phase

$$C_{MeO_i}^{SFMat_i} \Big|_{Dust} = (1 - \eta_{SFMat_i}) \cdot C_{MeO_i}^{SFMat_i} \tag{eq. 123}$$

$$C_{Me_i}^{SFMat_i} \Big|_{Dust} = (1 - \eta_{SFMat_i}) \cdot C_{Me_i}^{SFMat_i} \tag{eq. 124}$$

From carbonaceous materials

The eq. 125 to eq. 130 compute the partitioned mass concentrations regarding any grade of slag former materials.

$$W_{Source,t}^{Destination} = (r_t^{CMat_i} \cdot C_{Source,Me-MeO_i}^{CMat_i} \Big|_{Destination}) \cdot \Delta t \tag{eq. 125}$$

where *Destination*= Metal, Slag or Dust; *Source* = Rust, Impurities;

3.7.4.3. Partition of Carbonaceous Materials

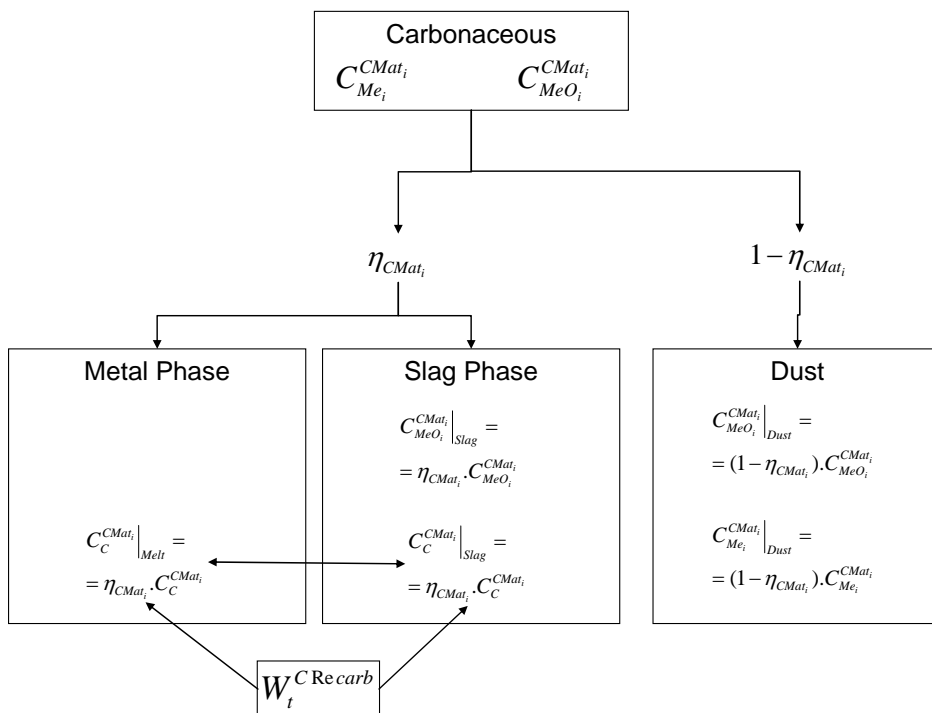


Figure 54 – Weight partition flow for elements and oxides content in the carbonaceous materials

The term $W_t^{C^{Re carb}}$, described subsequently in 3.13 section, is governed by a presumed equilibrium of iron oxide content in the slag phase and its relation with the carbon content in the metal phase.

To the metal phase

$$C_C^{CMat_i} \Big|_{Melt} = \eta_{CMat_i} \cdot C_C^{CMat_i} \quad \text{eq. 126}$$

To the slag phase

$$C_{MeO_i}^{CMat_i} \Big|_{Slag} = \eta_{CMat_i} \cdot C_{MeO_i}^{CMat_i} \quad \text{eq. 127}$$

$$C_C^{CMat_i} \Big|_{Slag} = \eta_{CMat_i} \cdot C_C^{CMat_i} \quad \text{eq. 128}$$

To the dust phase

$$C_{MeO_i}^{CMat_i} \Big|_{Dust} = (1 - \eta_{CMat_i}) \cdot C_{MeO_i}^{CMat_i} \quad \text{eq. 129}$$

$$C_{Me_i}^{CMat_i} \Big|_{Dust} = (1 - \eta_{CMat_i}) \cdot C_{Me_i}^{CMat_i} \quad \text{eq. 130}$$

3.7.5. Oxy-Reduction Reactions

During the EAF processing, oxy-reduction reactions can occur according to the thermodynamic equilibrium relations or even to the non-equilibrium relations.

Assumptions:

The Ellingham type diagram in Figure 55 shows the Standard Gibbs' free energy of the Fe and other tramp elements and their respective pure oxides [75]. At an EAF process temperature of 1600° C, ordering from the lowest to the highest affinity for oxygen results in: Cu, Ni, Sn, W, Mo, P, Fe, Zn, and Cr. In addition, other elements relevant to steelmaking, following the highest oxygen affinity order can be included to the list as Mn, Nb, V, Si, Ti, and Al. At an oxygen partial pressure of 10^{-8} bar, which normally prevails in the steel melt in equilibrium

with the slag during the steelmaking processes, only oxidation of Fe, Zn, Cr, Mn, Nb, V, Si, Ti, and Al would thus be possible at 1600° C. However, this approach is limited to pure elements in equilibrium with their pure oxides, which is not realistic in the steelmaking environment. Some of the mentioned tramp elements are present in the steelmaking process in dissolved and diluted form, while the oxides produced are also present in the slag in dilute form and may form complex compounds with other oxides. For instance, P and S removal is well known to be dependent of CaO, MgO, SiO₂ and Al₂O₃ content in the slag phase.

If the removal of tramp elements by means of oxidation and the formation of the corresponding oxides are not probable according to Ellingham diagram type, the weight of species like Cu, Ni, W, and Mo, are accounted as remaining residuals dissolve in the metal phase $W_{Re,s,t}^{Melt}$. As a matter of simplification, it is assumed that oxidation reaction is not occurring only for these elements.

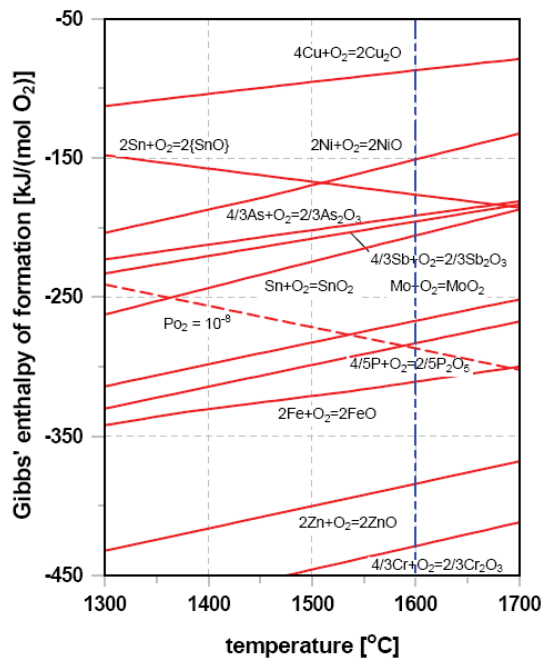


Figure 55 – Ellingham diagram for some of the usual tramp elements in steel [75].

Table 15 summarizes the assumptions adopted to simplify the mathematics effort to solve the multiple equations algorithm.

Table 15 – Reaction type and destination of elements and oxides

Specie Me_i	Reaction	Phase $Me_i \leftrightarrow W_t^{Me_i-Oxi}$
Al, Si, S	$-W_t^{Me_i-Oxi}$	Metal-Slag Phases
Zn		Dust Phase
Mn, P, Cr	$-W_t^{Me_i-Oxi} + W_t^{MeO_i-Red}$	Metal-Slag Phases
Nb, V, Ti		Neglected
C	$-W_t^{C-Oxi} + W_t^{CRecarb}$	Metal-Gas Phases
Fe	$-W_t^{Fe-Oxi} + W_t^{FeO-Red} - W_t^{FeVap}$	Metal-Slag-Dust Phases
Cu, Ni, W, Mo	Not Reacting	Metal-Phase

3.7.6. Metal Phase

The mass balance for Metal Phase (Metal Phase):

$$\begin{aligned}
 W_t^{Metal} &= & \text{eq. 131} \\
 &= W_{Fe,t}^{Metal} + W_{C,t}^{Metal} + \\
 &+ W_{Al,t}^{Metal} + W_{Si,t}^{Metal} + W_{Mn,t}^{Metal} + \\
 &+ W_{S,t}^{Metal} + W_{P,t}^{Metal} + W_{Cr,t}^{Metal} + W_{Res,t}^{Metal}
 \end{aligned}$$

The hot heel is assumed to be $W_0^{Heel} = W_t^{Metal}$ when $t=0$. Aluminum, Silicon, and Sulfur mass balances assume only oxidation reaction $-W_t^{Me_i-Oxi}$.

$$\begin{aligned}
 W_{Me_i,(t+\Delta t)}^{Metal} &= W_{Me_i,t}^{Metal} + \sum_{i=1}^n r_t^{FeMat_i} \cdot C_{Me_i}^{FeMat_i} \cdot \Delta t - & \text{eq. 132} \\
 &- W_t^{Me_i-Oxi}
 \end{aligned}$$

Equation eq. 133 emphasizes the difference in the melting rates of the scrap mix and the pig iron

$$\begin{aligned} \sum_{i=1}^n r_t^{FeMat_i} \cdot C_{Me_i}^{FeMat_i} \cdot \Delta t &= \text{eq. 133} \\ &= (r_t^{PIron} \cdot C_{Me_i}^{PIron} + \sum_{i=1}^n r_t^{Scrap_i} \cdot C_{Me_i}^{Scrap_i}) \cdot \Delta t \end{aligned}$$

Manganese, Phosphorus, Chromium mass balances assume oxy-reduction reactions $-W_t^{Me_i-Oxi} + W_t^{MeO_i-Red}$

$$\begin{aligned} W_{Me_i,(t+\Delta t)}^{Metal} &= W_{Me_i,t}^{Metal} + \sum_{i=1}^n r_t^{FeMat_i} \cdot C_{Me_i}^{FeMat_i} \cdot \Delta t - \text{eq. 134} \\ &- W_t^{Me_i-Oxi} + W_t^{MeO_i-Red} \end{aligned}$$

Carbon mass balance assumes oxidation $-W_t^{C-Oxi}$ and $W_t^{CRecarb}$ for metal phase re-carburization event that increases the soluble carbon in the Fe-C melt.

$$\begin{aligned} W_{C,(t+\Delta t)}^{Metal} &= W_{C,t}^{Metal} + \sum_{i=1}^n r_t^{FeMat_i} \cdot C_C^{FeMat_i} \cdot \Delta t - \text{eq. 135} \\ &- W_t^{C-Oxi} + W_t^{CRecarb} \end{aligned}$$

Iron mass balance assumes oxy-reduction $-W_t^{Fe-Oxi} + W_t^{Fe-Red}$ and vaporization reaction

$$\begin{aligned} W_{Fe,(t+\Delta t)}^{Metal} &= W_{Fe,t}^{Metal} + \text{eq. 136} \\ &+ \left(r_t^{FeMat_i} \cdot \left(C_{Fe}^{FeMat_i} + C_{Rust,Fe}^{FeMat_i} \Big|_{Metal} \right) \right) \Delta t - \\ &- W_t^{Fe-Oxi} + W_t^{FeO-Red} - W_t^{FeVap} \end{aligned}$$

where $C_{Rust,Fe}^{FeMat_i} \Big|_{Metal}$ is described in eq. 111. The term $W_t^{FeO-Red}$ refers to the iron oxide reduction, reverting Fe to the metal phase bulk. $-W_t^{FeVap}$ is later oxidized and addressed to the dust phase is described in 3.7.8 Dust Phase section.

The generic term W_t^{Me-Oxi} presented in eq. 132 to eq. 136 refers to the element weight at any time t which was consumed to produce oxide: $W_t^{Al-Oxi} \rightarrow Al_2O_3$, $W_t^{Si-Oxi} \rightarrow SiO_2$, $W_t^{Mn-Oxi} \rightarrow MnO$, $W_t^{P-Oxi} \rightarrow P_2O_5$, $W_t^{Fe-Oxi} \rightarrow FeO$,

$W_t^{C-Oxi} \rightarrow CO$ or CO_2 , and added to the slag phase or to the gas phase in the case of carbon oxidation.

The weight of an element Me_i oxidized from ferrous materials is equivalent to the difference of its input weight and its weight in equilibrium or non-equilibrium in the metal phase at anytime t . For instance, eq. 137 and eq. 138 are not considering the vaporization portion,

$$a.(Me - Oxi_i) + b.O_2 \leftrightarrow c.MeO_i \quad \text{eq. 137}$$

If the source of oxygen is enough to proceed the oxidation reaction, then

$$\begin{aligned} (-W_t^{Me_i-Oxi} + W_t^{MeO-Red}) = & \sum_{i=1}^n (W_t^{FeMat_i} \cdot C_{Me_i}^{FeMat_i}) - \\ & - \sum_{i=1}^n (W_t^{Melt} \cdot C_{Me_i}^{Melt}) \end{aligned} \quad \text{eq. 138}$$

If $(-W^{Me-Oxi} + W^{MeO-Red}) < 0$, the oxidation of iron is predominant. Otherwise, if $(-W^{Me-Oxi} + W^{MeO-Red}) > 0$, the reduction of iron oxide is predominant and iron moving back to the metal phase will occur.

In reference to $C_{Me_i t}^{Melt}$ for each of the Me_i listed, there is a corresponding code in Table AN1 - 11 such as L_{Me} , Min_{Me} or NR , meaning: partition coefficient, minimum content in equilibrium on tapping, and no reaction occurs, respectively. Hence, according to eq. 146 for L_{Mn_i} , eq. 151 for L_{P_i} , and eq. 153 for L_{Cr_i} , the $C_{Me_i t}^{Melt}$ can be computed respecting the partition coefficients L_{Me_i} of the element Me_{it} dissolved in the metal phase and its respective oxide $Me - Oxi_i$ dissolved in the slag $C_{MeO_i t}^{Slag}$ at anytime t . Thus, a general equation could be defined for the partition ratio L_{Me} ,

$$L_{Me} = \frac{C_{Me_i}^{Slag}}{C_{Me_i}^{Melt}} = \frac{W^{Me-Oxi_i}}{C_{Me_i}^{Melt}} \quad \text{eq. 139}$$

where,

$$W_{(t+\Delta t)}^{Me-Oxi_i} = W_t^{Me-Oxi_i} + r_t^{Me-Oxi_i} \cdot \Delta t \quad \text{eq. 140}$$

$$W_{(t+\Delta t)}^{Me-Oxi_i} = W_t^{Me-Oxi_i} + L_{Me_i} \cdot C_{Me_i}^{Melt} \cdot W_t^{Slag} \quad \text{eq. 141}$$

Removal or pickup of Nitrogen is ignored in the present model.

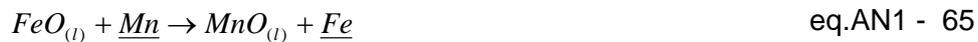
3.7.7. Slag Phase

The weight of oxides formed W_t^{Me-Oxi} due to reaction of Me_i with the injected oxygen, is added to the dissolve oxides content from other raw materials, and then, addressed to the slag phase.

$MeO_i \rightarrow Al_2O_3$ and SiO_2 weight

$$\begin{aligned} W_{MeO_i,t+\Delta t}^{Slag} &= W_{MeO_i,t}^{Slag} + \\ &+ \left(r_t^{Imp} \cdot C_{Imp}^{FeMat_i} \Big|_{Slag} \cdot C_{MeO_i}^{Imp} + r_t^{MeO_i} \cdot C_{MeO_i}^{SFMat_i} + r_t^{MeO_i} \cdot C_{MeO_i}^{CMat} \right) \Delta t + \\ &+ W_t^{Me-Oxi_i} \cdot \frac{MW_{MeO_i}}{MW_{Me_i}} \end{aligned} \quad \text{eq. 142}$$

MnO weight



$$W_{MnO,t+\Delta t}^{Slag} = W_{MnO,t}^{Slag} + W_t^{Mn-Oxi} \cdot \frac{MW_{MnO}}{MW_{Mn}} \quad \text{eq. 143}$$

arranging eq. AN1 - 68,

$$C_{Mn_i}^{Melt} = \frac{1}{K_{FeMn}} \frac{\gamma_{MnO}}{\gamma_{FeO}} \frac{X_{MnO}}{X_{FeO}} \quad \text{eq. 144}$$

K_{FeMn} is the equilibrium constant of reaction $FeO_{(l)} + Mn \rightarrow MnO_{(l)} + Fe$ (eq.AN1 - 64 and eq.AN1 - 65), $\gamma_{MnO}/\gamma_{FeO}$, is function of basicity index B, and X_{MnO}/X_{FeO} is the molar ratio of manganese and iron oxides. Thus, W_t^{Mn-Oxi} can be estimated,

$$K_{FeMn} = \frac{a_{MnO}}{a_{FeO} \cdot [\%Mn]} = EXP\left(\frac{15,766}{T} - 7.144\right) \quad \text{eq.AN1 - 66}$$

$$W_{(t+\Delta t)}^{Me-Oxi} = W_t^{Me-Oxi} + L_{Met} \cdot C_{Me_i}^{Melt} \cdot W_t^{Slag} \quad \text{eq. 145}$$

$$L_{Mn} = \frac{\%C_{Mn}^{Slag}}{\%C_{Mn}^{Melt}} = \frac{\%C_{MnO}^{Slag} \cdot \frac{MW_{Mn}}{MW_{MnO}}}{\%C_{Mn}^{Melt}} 2.77(\%C_{FeO}^{Slag}) \quad \text{eq. 146}$$

FeO weight

$$W_{FeO,t+\Delta t}^{Slag} = W_{FeO,t}^{Slag} + \left(r_t^{Rust} \cdot \left(C_{Rust,FeO}^{FeMat_i} \Big|_{Slag} \right) \Delta t + (W_t^{Fe-Oxi} - W_t^{Fe-Red}) \right) \frac{MW_{FeO}}{MW_{Fe}} \quad \text{eq. 147}$$

$(W_t^{Fe-Oxi} - W_t^{Fe-Red})$ is computed according to iron oxide reduction rate to be described in session 3.11 Iron Oxidation and Reduction Rate.

CaO weight

$$W_{CaO,t+\Delta t}^{Slag} = W_{CaO,t}^{Slag} + \left(\left(r_t^{Imp} \cdot \left(C_{Imp}^{Scrap} \Big|_{Slag} + C_{Imp}^{PIron} \Big|_{Slag} \right) C_{CaO}^{Imp} \right) + \left(r_t^{Flux} \cdot (\eta_{Lime} \cdot C_{CaO}^{Lime} + \eta_{Lime} C_{CaO}^{Dolo}) \right) \right) \Delta t \quad \text{eq. 148}$$

MgO weight

$$W_{MgO,t+\Delta t}^{Slag} = W_{MgO,t}^{Slag} + \left(\left(r_t^{Imp} \cdot \left(C_{Imp}^{Scrap} \Big|_{Slag} + C_{Imp}^{PIron} \Big|_{Slag} \right) C_{MgO}^{Imp} \right) + \left(r_t^{Flux} \cdot (\eta_{Lime} \cdot C_{MgO}^{Lime} + \eta_{Lime} C_{MgO}^{Dolo} + C_{MgO}^{Refrat}) \right) \right) \Delta t \quad \text{eq. 149}$$

P₂O₅ weight

$$L_P = f(C_{FeO}^{Slag}, C_{SiO_2}^{Slag}, C_{P_2O_5}^{Slag}) \quad \text{eq. 150}$$

$$\log L_P = \left(\begin{array}{l} \frac{10730}{T} + \\ + 4.11 \cdot \log(\% C_{CaO}^{Slag} + 0.15\% C_{MgO}^{Slag} - 0.05\% C_{FeO}^{Slag}) + \\ + 2.5 \cdot \log \% C_{FeO}^{Slag} + 0.5 \cdot \log \% C_{P_2O_5}^{Slag} - 13.87 \end{array} \right) \quad \text{eq. 151}$$

Cr₂O₃ weight

Assuming the chromium oxidation reaction in the system Fe-Cr-O could be represented by eq. 152 [8],



thus, eq. 153 and eq. 154 are proposed

$$L_{Cr} = \frac{C_{Cr}^{Slag}}{C_{Cr}^{Melt}} = 0.3(C_{FeO}^{Slag}) \quad \text{eq. 153}$$

$$C_{Cr_2O_3}^{Slag} = 0.3 \cdot C_{Cr}^{Melt} \cdot \frac{MW_{Cr_2O_3}}{2 \cdot MW_{Cr}} \cdot (C_{FeO}^{Slag}) \quad \text{eq. 154}$$

Consequently, the slag phase weight and chemical composition at any time t can be computed according to eq. 155 and eq. 156

$$W_t^{Slag} = \sum_{i=1}^n (W_t^{MeO_i}) - W_t^{SlagOff} \quad \text{eq. 155}$$

where $W_t^{SlagOff}$ is the weight of slag which is removed from the EAF, which rate will be described in session 3.12 Slag Off Rate.

$$C_{MeO_i,t}^{Slag} = \frac{W_t^{MeO_i}}{\sum_{i=1}^n W_t^{MeO_i}} \quad \text{eq. 156}$$

3.7.8. Dust Phase

The “Dust” weight at any time t is expressed by eq. 157.

Dust mass balance

$$W_{t+\Delta t}^{Dust} = W_t^{Dust} + \left[\begin{aligned} & r_t^{Imp} \cdot \left(C_{Rust,Fe}^{PIron} \Big|_{Dust} + C_{Rust,FeO}^{PIron} \Big|_{Dust} + C_{Imp}^{PIron} \Big|_{Dust} \right) + \\ & + r_t^{Imp} \cdot \left(C_{Rust,Fe}^{Scrap} \Big|_{Dust} + C_{Rust,FeO}^{Scrap} \Big|_{Dust} + C_{Imp}^{Scrap} \Big|_{Dust} \right) + \\ & + (1 - \eta_{Lime} + 1 - \eta_{Dolo}) \cdot r_t^{Flux} \end{aligned} \right] \cdot \Delta t \quad \text{eq. 157}$$

3.7.9. Gas Phase

The gas phase is computed partially consisting of CO, CO₂, H₂O and O₂. Other compounds such as N₂, H₂, NO_x (N oxides) and complex hydrocarbon compounds are not taken into account in this study. The flow rate of CO, Q_{CO} , is produced by the direct carbon oxidation reaction both from dissolved carbon in iron and from carbonaceous materials like coke. Further, Q_{CO_2} , the flow rate of CO₂, is influenced by the reaction from post combustion of CO, as well the additional portion of CO₂ which is produced during natural gas oxidation. Slag formers are presumed fully calcinated, hence, they are not considered as a source of CO₂. The flow rate of H₂O, Q_{H_2O} , can be produced from natural gas oxidation and from moisture that might be present in ferrous materials.

Therefore, the simplified off-gas volume flow rate can be described by eq. 158.

$$Q^{OffGas} = Q_{O_2}^{OffGas} + Q_{CO} + Q_{CO_2} + Q_{H_2O} \quad \text{eq. 158}$$

The infiltration gas from the surrounding atmospheric air is the main source of the total off-gas volume. The off-gas system produces negative pressure in the EAF internal volume in order to exhaust dust present at or formed from the charged solid materials, and the oxidation gases for environmental issues and safety purposes. However, the EAF is not completely sealed, since the auxiliary devices, which are introduced into the EAF volume during steelmaking process, require openings. For instance, slag door open area, holes for electrodes, misalignment of upper shell and roof are usual “gaps” that contribute for infiltration air. In spite of oxygen content in the infiltrated air could react with the charged solid ferrous and carbonaceous materials, it is presumed to exert a minor influence and is not accounted in the metal, slag, dust nor gas phases.

3.7.9.1. Oxygen Mass Balance

The present model computes only four sources of reactive oxygen, which are input and react with species dissolved in iron: (i) Lance injector $N_{O_2}^L$, (ii) Post combustion injector $N_{O_2}^{PC}$, (iii) Burner injector $N_{O_2}^{Burners}$ and (iv) dissolution of FeO content in the rust is represented by $N_{O_2}^{FeO}$, described by eq. 99. Oxygen molar rate due to any non reacted oxygen and oxygen content in resultant gases CO and CO₂ are represented by $N_{O_2}^{OffGas}$. All the slag formers are presumed to not change their oxygen content, therefore, $N_{O_2}^{Slag}$ denotes only oxides created by oxidation of Si, Mn, P, Al, Cr and Fe which are addressed to the slag phase. $N_{O_2}^{Metal}$ is a minor portion of oxygen which is dissolved in iron melt. From mass conservation premise,

$$N_{O_2}^L + N_{O_2}^{PC} + N_{O_2}^{Burners} + N_{O_2}^{FeO} = N_{O_2}^{Slag} + N_{O_2}^{Metal} + N_{O_2}^{OffGas} \quad \text{eq. 159}$$

other sources of oxygen are considered negligible.

The dissolved FeO in the slag can react with carbon, if there is available carbon in the slag phase and the equilibrium condition is not favorable for recarburization. The current model considers FeO reacting with carbon in the slag, even though there is the possibility to react with dissolved carbon in metal

phase. Actually, for computing simplification, the model accounts for oxygen consumption first through the reaction with Al, Si, Cr, Mn and C, and the excess is consumed to create FeO at every time interval Δt applied to the numeric integration.

The efficiency of the injected oxygen to react with metal and gaseous phases is presumed to be lower than 100%, influenced by different injection technologies available in EAF facilities (Figure 57). In terms of the injected oxygen volume flow rate, $N_{O_2}^k$ is now replaced by $Q_{O_2}^k$ [$\text{Nm}^3\text{O}_2/\text{h}$], and such coefficients are defined below to take into account different efficiencies.

Regarding the lancing mode, eq. 160 describes the oxygen flow rate in excess that will react and create FeO, $Q_{O_2}^{L,excess}$, which is the oxygen available from the Lance injectors after reactions with C, Si, Mn, Al, P and Cr in the metal phase. OLE_{FeO} coefficient defines the percentage of $Q_{O_2}^{L,excess}$ reacting with iron, resulting in $Q_{O_2}^{L,FeO}$, the net oxygen flow rate reacting with iron (eq. 161).

$$Q_{O_2}^{L,excess} = Q_{O_2}^L - \sum Q_{O_2}^{L,Me_i} \quad \text{eq. 160}$$

$$Q_{O_2}^{L,FeO} = Q_{O_2}^{L,excess} \cdot OLE_{FeO} \quad \text{eq. 161}$$

The role of post combustion injectors has been controversial over the years. Depending on the flow rate, location in EAF and the infiltration air flow rate, the PC injectors can present multifunction behavior. The oxygen flow rate reacting with CO is defined as $Q_{O_2}^{PC,CO}$ according to the PCR setting.

In similar manner to lance injectors, it is assumed that excess of oxygen $Q_{O_2}^{PC,excess}$ injected through post combustion injectors that does not produce CO oxidation could decarburize the metal phase too, even though it is not its original purpose. For instance, during the meltdown, if there is significant amount of solid scrap in the EAF, the oxygen from PC injectors may oxidize the scrap surface. Later, the scrap falls from the EAF walls and react with soluble carbon in the metal phase. Thus, the coefficient $OPCE_{Decarb}$ estimates how much additional oxygen coming from PC injectors will be taken into account for decarburization mode $Q_{O_2}^{PC,Decarb}$.

$$Q_{O_2}^{PC,excess} = Q_{O_2}^{PC} - Q_{O_2}^{PC,CO} \quad \text{eq. 162}$$

$$Q_{O_2}^{PC,Decarb} = Q_{O_2}^{PC,excess} \cdot OPCE_{Decarb} \quad \text{eq. 163}$$

Actually, $Q_{O_2}^{PC,Decarb}$ is reacting also with Al, Si, Mn, P, Cr besides C, up to their minimum content in metal phase. If the minimum contents of the referred species are attained, any remaining oxygen is accounted for FeO creation at every time interval Δt . Hence, $OPCE_{FeO}$ coefficient is defined as the percentage of the oxygen available from the post combustion injectors that creates iron oxide both in the solid ferrous materials and in the metal phase, after CO oxidation above the slag line and other species oxidation.

$$Q_{O_2}^{PC,excess} = Q_{O_2}^{PC} - Q_{O_2}^{PC,CO} \quad \text{eq. 164}$$

$$Q_{O_2}^{PC,FeO} = (Q_{O_2}^{PC,excess} - Q_{O_2}^{PC,Decarb}) \cdot OPCE_{FeO} \quad \text{eq. 165}$$

As a result, eq. 166 estimates the remaining oxygen balance available for iron oxidation. It is assumed that the oxygen content in the infiltration air is not reacting with any phase.

$$Q_{O_2}^{Fe-FeO} = Q_{O_2}^{L,excess} \cdot OLE + (Q_{O_2}^{PC,excess} - Q_{O_2}^{PC,Decarb}) \cdot OPCE_{FeO} \quad \text{eq. 166}$$

Thus, eq. 167 estimates the oxygen flow rate which is not reacting in the EAF and flows away through the off-gas system,

$$Q_{O_2}^{OffGas} = Q_{O_2}^{L,excess} \cdot (1 - OLE) + Q_{O_2}^{PC,excess} \cdot (1 - OPCE_{Decarb} - OPCE_{FeO}) + B_{excess} \cdot Q_{NG} \quad \text{eq. 167}$$

in the case of burners, the oxygen required for complete combustion is defined by,

$$Q_{O_2}^{Burners} = (2 + B_{excess}) \cdot Q_{NG} \quad \text{eq. 168}$$

where, $(2 + B_{excess})$ means the additional oxygen for the stoichiometry from eq. 90, and Q_{NG} is the natural gas flow rate.

The coefficients computing oxygen efficiencies are estimated through inverse calculation.

3.8. Decarburization Rate Model

It is well accepted that the decarburization reaction occurs by oxygen first reacting with iron to form FeO in slag. Then carbon diffuses in the metal to the interface of reaction slag-metal, reducing FeO and producing CO as indicated by the following reactions described on eq.AN1 - 30 and eq.AN1 - 47,



The decarburization kinetics of Fe-C melt has been proved to occur in two different patterns [1-4, 9, 11], connected by a common carbon content known as the critical carbon content, when a transition of decarburization mechanism takes place. Above the critical carbon, the driving force for mass transfer of carbon is sufficient to reduce all of the FeO formed. Hence, the decarburization rate is independent of carbon content and influenced only by the oxygen availability or flow rate, as described by eq. 169 which is derived from eq.AN2 - 31:

$$\left. \frac{d[\%C]_t}{dt} \right|_{\%C > \%C^{Cr}} = r_t^{C-Ox_i} = -c \cdot \frac{MW_C}{W_t^{Metal}} (2 - R_{PC}^{Melt}) \cdot 100 \cdot Q_{O_2,t}^{L*} \quad \text{eq. 169}$$

Where R_{PC} is the post combustion ratio, c is conversion factor from molar to volume flow rate (Nm^3), W_t^{Metal} is the weight of liquid metal phase at time t , $Q_{O_2,t}^{L*}$ is the oxygen injection rate at time t through lance injectors and PC injectors available for decarburization, and MW_C is the molecular weight of carbon.

$$R_{PC} = \frac{\%CO_2}{\%CO_2 + \%CO} \quad \text{eq. 170}$$

From eq.AN2 - 37, $(2 - R_{PC}^{Metal})$ is equivalent to $(1 + F_{CO})$

$$\frac{d[\%C]}{dt} = -c \cdot \frac{MW_C}{W_t^{Metal}} \cdot (1 + F_{CO}) \cdot 100 \cdot Q_{O_2,t}^{L*} \quad \text{eq.AN2 - 37}$$

$$F_{CO} = \frac{\%CO}{\%CO_2 + \%CO} \quad \text{eq. 171}$$

The gas phase is taken upon following ideal gas behavior, the total pressure is 1 atm, the partial pressure of CO p_{CO} is presumed equivalent to X_{CO} , its molar fraction in the gas phase. Even though some authors assume R_{PC} negligible ($F_{CO} \equiv 1.0$), the current model applies eq.AN1 - 27. The molar fraction X_{CO} may varies from 0.93 to 0.98 when soluble carbon in Fe-C melt are 0.02% and 0.10%, respectively

$$\frac{X_{CO}^2}{1 - X_{CO}} = EXP\left(\frac{-17.802}{T} + 15,90\right) \cdot f_c \cdot [\%C] \quad \text{eq.AN1 - 27}$$

The non-reacted CO can be further oxidized to CO_2 by post combustion [76, 77] in the furnace gas phase above the slag surface, where no graphite is available, according to eq.AN1 - 62.



Below the critical carbon, the carbon mass transfer rate decreases and not all of the FeO are reduced, and actually, its content in the slag tends to increase. Therefore, the decarburization rate is controlled by liquid phase mass transfer of carbon as expressed by eq.AN2 - 43.

$$\left. \frac{d[\%C]_r}{dt} \right|_{\%C < \%C^{Cr}} = r_t^{C-Ox_2} = -\frac{\rho^{Melt} m_C \cdot A}{W_t^{Metal}} ([\%C]^\infty - [\%C]^{eq}) \quad \text{eq.AN2 - 43}$$

where, m_C is the liquid phase mass transfer coefficient of carbon in iron metal phase, A is the interfacial area where the decarburization occurs, ρ^{Metal} is the density of metal phase, and R_{PC} is the post combustion ratio. The minimum carbon content in equilibrium $[\%C]^{eq}$ is assumed negligibly small by some authors compared to the carbon content in the metal phase. However for the current model, an empirical limit for $[\%C]^{eq}$ assumes the value of 0.03%.

Considering W_t^{Metal} constant when all the charge is fully melted, equating eq.AN2 - 37 and eq.AN2 - 43, the critical carbon content can be computed,

$$[\%C]^{Cr} = c \cdot \frac{MW_C}{\rho^{Metal} m_C A} \cdot (1 + F_{CO}) \cdot 100 \cdot Q_{O_2,t}^{L*} + [\%C]^{eq} \quad \text{eq. 172}$$

For $[\%C] > [\%C]^{Cr}$

$$\left. \frac{d[\%C]_t}{dt} \right|_{\%C > \%C^{Cr}} = r_t^{C-Ox_i} = -k_{C1} \cdot Q_{O_2,t}^{L*} \quad \text{eq. 173}$$

$$k_{C1} = c \cdot \frac{MW_C}{W_t^{Metal}} \cdot (1 + F_{CO}) \cdot 100 \quad \text{eq. 174}$$

k_{C1} [1/Nm³]

$$\begin{aligned} -W_t^{C-Ox_i} \Big|_{\%C > \%C^{Cr}} &= r_t^{C-Ox_i} \Big|_{\%C > \%C^{Cr}} \cdot \Delta t \cdot W_t^{Metal} \\ &= -c \cdot MW_C \cdot (1 + F_{CO}) \cdot 100 \cdot Q_{O_2,t}^{L*} \cdot \Delta t \cdot W_t^{Metal} \end{aligned} \quad \text{eq. 175}$$

For $[\%C] < [\%C]^{Cr}$

$$\left. \frac{d[\%C]_t}{dt} \right|_{\%C < \%C^{Cr}} = r_t^{C-Ox_i} \Big|_{\%C < \%C^{Cr}} = -k_{C2} \cdot ([\%C]_t - [\%C]^{eq}) \quad \text{eq. 176}$$

$$k_{C2} = \frac{\rho^{Metal} m_C A}{W_t^{Metal}} \quad \text{eq. 177}$$

k_{C2} [1/min]

$$\begin{aligned} -W_t^{C-Ox_i} \Big|_{\%C < \%C^{Cr}} &= r_t^{C-Ox_i} \Big|_{\%C < \%C^{Cr}} \cdot W_t^{Melt} \cdot \Delta t = \\ &= -\rho^{Metal} m_C \cdot A \cdot ([\%C]_t - [\%C]^{eq}) \cdot \Delta t \end{aligned} \quad \text{eq. 178}$$

The critical carbon can be estimated equating eq. 173 and eq. 176

$$\left. \frac{d[\%C]_t}{dt} \right|_{\%C > \%C^{Cr}} = \left. \frac{d[\%C]_t}{dt} \right|_{\%C < \%C^{Cr}} \quad \text{eq. 179}$$

combining,

$$c \cdot \frac{MW_C}{W_t^{Metal}} \cdot (1 + F_{CO}) \cdot 100 \cdot Q_{O_2,t}^{L*} = \frac{\rho^{Metal} m_C A}{W_t^{Metal}} \cdot ([\%C]_t - [\%C]^{eq}) \quad \text{eq. 180}$$

At the transition point, $[\%C]_t = [\%C]^{Cr}$, thus $(m_c A)_t$ can be described by eq. 181,

$$(m_c A)_t = c \cdot \frac{MW_C (1 + F_{CO}) \cdot Q_{O_2,t}^{L*}}{\rho^{Metal} \cdot ([\%C]^{Cr} - [\%C]^{eq})} \quad \text{eq. 181}$$

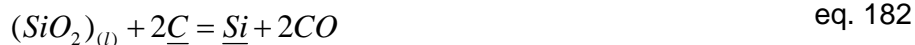
The value of the parameter “ $m_c A$ ” is usually obtained by measuring the rate of decarburization in the furnace, and then back calculating. Indeed, estimate of “ $(m_c A)_t$ ” is not easily available in the literature even for OSM operations, less is known for the EAF case. It is assumed that the parameter “ $(m_c A)_t$ ” is proportional to the oxygen flow rate in OSM. It is said to be approximately equivalent to 0.3% mass [9, 78] for OSM operations .

3.9. Desiliconization Rate Model

The effect of silicon may not be neglected due to the high contents in pig iron. Besides, it is still not well understood the fact that decarburization can take place even with %Si higher than the %Si minimum [12, 79].

Equilibrium between Fe-Si-O is assumed (eq. 183) instead of C-Si-O (eq. 182), because three-phase equilibrium is too slow and probably not achieved:

for slag-metal-gas system



and slag-metal system



The model for silicon removal rate, or desiliconization according to the reaction described in eq. 183, is assumed to be similar to the decarburization model [80],[81] regarding the existence of two regimes, I and II, connected by a critical silicon content. No gas phase is involved and the interfacial reaction is assumed to be in local equilibrium because of high reaction rate at elevated temperatures. Since the mass transfer of oxygen and silicon in the metal phase

are the controlling mechanism for regimes I and II, respectively, described by eq. 184 to eq. 189.

For $[\%Si] > [\%Si]^{Cr}$

$$\left. \frac{d[\%Si]_t}{dt} \right|_{\%Si > \%Si^{Cr}} = r_t^{Si-Oxi_1} = -k_{Si1} \cdot 100 \cdot Q_{O_2,t}^{L*} \quad \text{eq. 184}$$

$$k_{Si1} = c \cdot \frac{MW_{Si}}{W_t^{Metal}} \cdot 100 \quad \text{eq. 185}$$

k_{Si1} [1/Nm³]

$$\begin{aligned} -W_t^{Si-Oxi_1} \Big|_{\%Si > \%Si^{Cr}} &= r_t^{Si-Oxi_1} \Big|_{\%Si > \%Si^{Cr}} \cdot \Delta t \cdot W_t^{Metal} \\ &= -c \cdot MW_{Si} \cdot Q_{O_2,t}^{L*} \cdot \Delta t \cdot W_t^{Metal} \end{aligned} \quad \text{eq. 186}$$

For $[\%Si] < [\%Si]^{Cr}$

$$\left. \frac{d[\%Si]_t}{dt} \right|_{\%Si < \%Si^{Cr}} = r_t^{Si-Oxi_2} = -k_{Si2} \cdot ([\%Si]^\infty - [\%Si]^{eq}) \quad \text{eq. 187}$$

$$k_{Si2} = \frac{\rho^{Metal} m_{Si} A}{W_t^{Metal}} \quad \text{eq. 188}$$

k_{Si2} [1/min]

$$\begin{aligned} -W_t^{Si-Oxi_2} \Big|_{\%Si < \%Si^{Cr}} &= r_t^{Si-Oxi_2} \Big|_{\%C < \%C^{Cr}} \cdot \Delta t = \\ &= -\rho^{Metal} m_{Si} \cdot A \cdot ([\%Si]_t - [\%Si]^{eq}) \cdot \Delta t \end{aligned} \quad \text{eq. 189}$$

Similarly to decarburization model, $(m_{Si}A)_t$ can be estimated as,

$$\left. \frac{d[\%Si]_t}{dt} \right|_{\%Si > \%Si^{Cr}} = \left. \frac{d[\%Si]_t}{dt} \right|_{\%Si < \%Si^{Cr}} \quad \text{eq. 190}$$

rearranging,

$$(m_{Si}A)_t = c \cdot \frac{MW_{Si} \cdot Q_{O_2,t}^{L*}}{\rho^{Metal} \cdot ([\%Si]^{Cr} - [\%Si]^{eq})} \quad \text{eq. 191}$$

ThermoCalcTM estimates $[\%Si]^{eq}$ as virtually zero at EAF tapping conditions.

3.10. Dephosphorization Rate Model

The dephosphorization reaction consists of a complex interaction of slag and metal phases. Many studies and several kinetic-thermodynamic models have been developed and published in literature [72, 82-87]. Even though the present study is focused on the decarburization and iron oxide reduction rates, the phosphorus content is a valuable secondary indicator or tracer, with the purpose to support the pig iron melting rates estimates, as well the level of iron oxide present in the slag.

A brief description of the model adopted is presented below, starting with the assumption of phosphate compound and phosphorus mass transfer rate controlling mechanism, in slag and metal phases. The recent literature [72, 85-87] is in agreement that slag-metal phosphorus reaction can be described as,



Assuming that most of chemical reactions at slag-metal interface are fast at high temperatures involved in EAF processing, kinetic of phosphorus mass transfer is a candidate to be the rate controlling mechanism. The partition of phosphorus at slag (%P) and metal [%P] interface L_p proposed in eq. 151 points out the dependence of phosphorus equilibrium and the oxygen potential, represented by the FeO content in the slag phase. Several authors suggested that the oxygen feeding rate to the interface by the slag is faster than the mass transfer in the metal phase [83-85]. Hence, the kinetic of phosphorus oxidation and reversion are proposed to be controlled by mass transfer in the metal and slag phases, respectively, and described by eq. 193 and eq. 194 [72].

$$\left. \frac{d[\%P]_t}{dt} \right| = r_t^{P-Oxi} = -k_p \cdot ([\%P]^\infty - [\%P]^{eq}) \quad \text{eq. 193}$$

$$[\%P]^{eq} = \frac{(\%P)}{L_p}$$

$$k_p = \frac{\rho^{Metal} m_p^* A}{W_t^{Metal}} = \frac{\rho^{Metal} A}{W_t^{Metal}} \frac{1}{\left(\frac{\rho^{Metal}}{k_p^{Slag} \cdot \rho^{Slag} \cdot L_p} + \frac{1}{k_p^{Metal}} \right)} \quad \text{eq. 194}$$

For the sake of simplification, k_p is the overall rate parameter, accounting both mass transfer coefficient of phosphorus in the slag k_p^{Slag} and in the metal k_p^{Metal} phases. Mass transfer in both phases competes and the direction of reaction is dictated by the equilibrium at the interface of reaction.

3.11. Iron Oxidation and Reduction Rate

When soluble carbon content in the Fe-C melt decreases below the critical carbon, the iron oxidation becomes dominant and iron oxide maybe enriched in the slag phase, if there is no other source of simultaneous carbon input. Iron oxidation and decarburization are competitive reactions and the proportion between them is determined by the carbon source as described by $Fe_{(l)} + 1/2O_{2(g)} \rightarrow FeO_{(l)}$ (eq.AN1 - 30) and $FeO_{(l)} + \underline{C} = Fe + CO$ (eq.AN1 - 47). The amount of FeO produced and accounted for the slag is determined from the oxygen injected minus any oxygen used for metal phase decarburization, post combustion and the oxidation of other soluble elements (Al, Si, Mn, etc). Besides, in the EAF, part of the oxygen reacts directly with the solid scrap producing FeO, and as the scrap melts, the produced FeO heads to the slag phase or can be also carried out by the off-gas system as described previously at sessions 3.7.7 and 3.7.8 .

In the EAF operation, carbonaceous materials such as coke or anthracite can be used to compensate excess of oxygen injection and for slag foaming. It can be charged mixed with the scrap in the bucket and batch loaded in the EAF vessel. However, injected coke into the slag to reduce iron oxide for foaming slag is the most usual way for carbon input.

The overall reaction presented in eq.AN1 - 43 is resultant of reactions eq.AN1 - 30 and eq.AN1 - 3.



The iron oxidation rate presented in eq. 195 is assumed proportional to the oxygen flow rate available after primary consumption described in 3.7.9.1.

$$r_t^{Fe-Oxi} = c \cdot Q_{O_2,t}^{L*} \cdot 2 \cdot MW_{Fe} \quad \text{eq. 195}$$

thus, the iron weight oxidized to iron oxide W_t^{Fe-Oxi} can be estimate as

$$W_t^{Fe-Oxi} = r_t^{Fe-Oxi} \cdot \Delta t = c \cdot Q_{O_2,t}^{L*} \cdot 2 \cdot MW_{Fe} \cdot \Delta t \quad \text{eq. 196}$$

The model presumes that reaction described in eq. AN1 - 47, is a first order reaction in respect to carbon as well to iron oxide concentrations in the slag.



Thus, the empirical expression can be written as eq. 197, where $\alpha=\beta=1$,

$$r_t^{Fe-Red} = k_{Fe-Red}^{CMInj} \cdot (\% FeO_{(l)})^\alpha \cdot (\% C)^\beta \quad \text{eq. 197}$$

and combining $(\% C)^{Slag} = W_{C,t}^{Slag} / W_t^{Slag}$ in eq. 197,

$$\frac{d(\% FeO_{(l)})}{dt} \cdot W_t^{Slag} = k_{Fe-Red}^{CMInj} \cdot W_{C,t}^{Slag} \cdot (\% FeO_{(l)}) \quad \text{eq. 198}$$

It is proposed that the reduction rate of iron oxide occur as presented in eq. 199. This equation assumes that the rate r_t^{Fe-Red} is controlled by mass transfer of FeO in the slag and/or chemical kinetics, and the reaction area is proportional to the carbon weight in the slag $W_{C,t}^{Slag}$.

$$r_t^{Fe-Red} = k_{Fe-Red}^{CMInj} \cdot W_{C,t}^{Slag} \cdot \frac{((\% FeO)_t - (\% FeO^i)_t)}{100} \quad \text{eq. 199}$$

where k_{Fe-Red}^{CMInj} is the reaction rate constant, $W_{C,t}^{Slag}$ the mass of carbon in the slag. The weight of carbon injected in the slag in any time t can be computed according to eq. 200 and eq. 201.

$$W_{C,t}^{Slag} = W_{CM,t}^{Slag} \cdot C_C^{CM} \quad \text{eq. 200}$$

$$W_{CM,t}^{Slag} = \eta_{CMInj} \cdot r_t^{CMInj} \cdot \Delta t \quad \text{eq. 201}$$

where r_t^{CMInj} is the carbonaceous material injection rate. Hence, the balance for carbonaceous material in slag is calculated by eq. 202

$$W_{CM,t+\Delta t}^{Slag} = W_{CM,t}^{Slag} + \left(r_t^{CM} - r_t^{Fe-Red} \cdot \frac{MW_C}{MW_{FeO}} \right) \cdot \Delta t \quad \text{eq. 202}$$

The driving force for iron oxide reduction is a function of $((\%FeO)_t - (\%FeO^i)_t)$, where $(\%FeO^i)_t$ is the equilibrium of iron oxide mass concentration at slag-gas interface, usually assumed virtually zero.

Considering the equilibrium in the system Fe-C-O, whenever $(\%FeO)_t = (\%FeO^{eq*})_t$ is achieved, the available and non-reacted carbon in the slag will dissolve in the Fe-C melt instead, leading to subsequent FeO reduction according to FeO-C equilibrium curve, further described in session 3.13

3.12.

Slag Off Rate

Slag off usually occurs when the EAF vessel is tilted backward and/or the slag foam high enough to go over the slag door level. When iron oxide reaction with carbon produces proper CO flow rate and the slag viscosity fulfill the foaming requirements, the slag volume can increase more than four times its regular volume. Some extreme foaming conditions result in slag volume so huge, that slag off takes place through the electrodes holes in the EAF roof. As a matter of simplification, the current algorithm estimate slag off rate as a function of carbon injection flow rate,

$$W_t^{Slag-Off} = a \cdot r_t^{CMInj} \cdot t \quad \text{eq. 203}$$

3.13.

Re-Carburization

Recarburization is not an usual practice in EAF facilities focused in high productivity operations, due to its endothermic nature, which implies in higher energy consumption and longer processing time. However, particular experimental conditions conducted in this study could result in low FeO content in

the slag, low soluble oxygen level, and consequently, recarburization of metal phase could take place. The current algorithm does not account for carbonaceous particles injected directly in the metal phase, as represented in Figure 56 (a) and (b), even though such conditions might occur if the carbon injection flow rate is too high, and/or if the consumable pipe is deeply submerged in the metal phase. If the compressed air flow rate is adjusted for soft blowing (less than 100 Nm³/h) and kept constant by automation control, the carbonaceous particles tend to react mostly in the slag phase. Secondly, the steel pipe even though calorized, does not last long when submerged in the metal phase. Actually, the operators are inclined to keep the pipe wet by a protective slag and decrease significantly its consumption. Nevertheless, the boiling effect of CO generation and the emulsion formation, can make carbonaceous particles to go below the slag-metal phase interface.

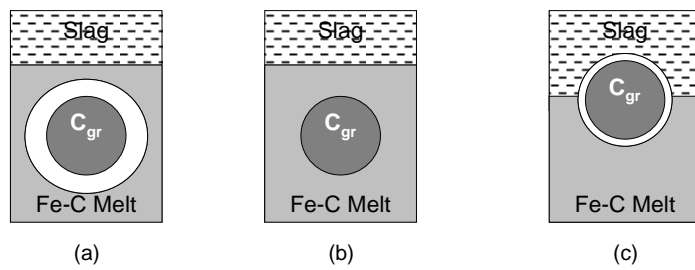


Figure 56 – Schematic representation of carbonaceous particle immersed (a) in Fe melt with high soluble oxygen; (b) neglected CO production and recarburization reaction takes place; (c) slag-metal interface.

Previous studies on carbon dissolution in Fe-C melts conducted elsewhere [88-92] have pointed out mass transfer of carbon in the liquid boundary layer adjacent to the solid particle, as the rate controlling mechanism. In addition, other factors like mineral structure, ash, carbon, and sulfur contents were reported to be influencing carbon dissolution rate. Ash, basically 70%SiO₂- 12%Fe₂O₃- 10%Al₂O₃-8%(Ca,Mg)O, decreases the carbon dissolution rate due to physical effect such as barrier formation and change on interfacial wettability. Surfacing effect of sulfur makes carbon dissolution to decrease. This effect has been relevant for sulfur contents higher than usually found in scrap based steelmaking (0.010% - 0.060%). For instance, negligible difference was found when sulfur content in the metal phase was in the range of 0-0.1%.

The carbonaceous material used in this study is known as calcinated petroleum coke, obtained from oil refinery units through cracking processes. Further calcination step improve the coke quality, providing high fixed carbon (90-

93%), low sulfur content (<1%), low ash content (0-3%), low volatiles (<10%), and low moisture (<1%). The proposed dissolution model applied to the current algorithm presumes carbon mass transfer as the rate controlling mechanism. The chemical reaction described in eq. 204 is assumed to be very fast.

$$C_{gr} = \underline{C} \quad \text{eq. 204}$$

Therefore, the molar rate of carbon dissolution reaction is described in eq. 205, where C_C^{Sat} and C_C are the molar concentration of carbon saturation in Fe-C melts and in the metal phase bulk at any time t .

$$\begin{aligned} N_{C_{gr}} &= -\frac{1}{A_t} \cdot \frac{dn_{C_{gr}}}{dt} = \\ &= N_C = -\frac{1}{A_t} \cdot \frac{dn_C}{dt} = -m_C \cdot (C_C^{Sat} - C_C) \end{aligned} \quad \text{eq. 205}$$

In terms of mass concentration, eq. 205 can be written according to eq. 206, where k_{ReC} is the rate constant. The driving force is governed by the difference of the saturation carbon content $[\%C]_{Sat}$ and the bulk carbon content $[\%C]_t$ in the metal phase at any time t . In similar way proposed to iron oxide reduction rate, the interface of carbon dissolution reaction is presumed to be proportional to the carbonaceous materials present in slag. Hence, eq. 206 can be written,

$$\left. \frac{d[\%C]_t}{dt} \right|_{ReC} \cdot W^{Metal} = r_t^{ReC} = -k_{ReC} \cdot W_{C,t}^{Slag} \cdot \left(\frac{[\%C]_{Sat} - [\%C]_t}{100} \right) \quad \text{eq. 206}$$

As a matter of simplification, carbonaceous materials is presumed in spherical geometry; shrinking core model without ash layer formation [93] (Figure AN2 - 2). For calculation convenience, recarburization rate is written in terms of conversion rate vs. time

$$Conversion = F_t^{CMatCh} = \frac{W_i - W_{p,t}}{W_i} =$$

$$= \frac{W_i - \left(W_i^{1/3} - \left(\frac{Y}{\rho^{gr}} \right)^{2/3} \cdot \rho^{Melt} \cdot m_C \cdot (\% C_{Sat} - \% C) \cdot t \right)^3}{W_i} \quad \text{eq.AN2 - 81}$$

$$Y = \left(\frac{4}{3} \pi \right)^{1/2} \quad \text{eq.AN2 - 80}$$

3.14. Model Parameters Determination

Instead of using only data from literature or setting values for most of the unknown parameters, the proposed model was submitted to an inverse calculation through an optimization algorithm. There are 19 parameters to be estimated to fulfill the proposed model demands. Therefore, a generalized reduced gradient algorithm (GRG) was applied to estimate the unknown parameters. GRG algorithm was applied for optimization of linear constrained and non linear systems. By varying the model parameters, calculation of the deviation between measured values and the predicted values can be minimized. This approach is similar to regression methods and often called inverse modeling [94]. The GRG objective function presented in eq. 207 was defined for minimization of the differences between the model prediction and the experimental results regarding: C in the metal phase and for CaO, MgO, SiO₂, FeO in the slag composition.

Therefore, chemical analysis are required for the slag samples including CaO, MgO, SiO₂, Al₂O₃, P₂O₅, Cr₂O₃ and FeO, and for steel samples, for C, Si, Mn, S and P.

$$\text{Objective Function} = \sum_{i=\text{Substance}} \left| \% Conc_i^{\text{model}} - \% Conc_i^{\text{experimental}} \right| \cdot p_i \quad \text{eq. 207}$$

where,

$$\% Conc_i = [\% C]_{\text{Steel}}; (\% FeO, \% CaO, \% SiO_2, \% MgO)_{\text{Slag}}$$

p_i is the weight given for each of the selected species, resulting in different priorities for the optimization algorithm. For the current project, the %FeO and %C were chosen as the most important species, followed by CaO, SiO₂ and MgO.

The primary parameters, are related directly to the reactions phenomenology: k_{C1} and k_{C2} , as the decarburization constants, k_{red} reduction rate constant of FeO by injected carbon, R_{PC} post combustion ratio. The secondary parameters consisted of operational parameters which are usually difficult to measure, such as melting rates, the amount of oxygen in excess which is indeed reacting, the amount of formed slag and also, the particular set of reactions that may represent more significant participation of different kinds of oxygen injectors.

3.15. Process Model Summary

The model includes the rate phenomena for decarburization and C-FeO reaction in the slag, mass balance for usual species carried by commercial ferrous materials in the metal, slag and gas phases.

- The changes along the processing time of the carbon content in the metal phase and the slag chemistry are computed by the model;
- The model can be used to predict iron yield and carbon loss with the discharged slag;
- Mass balance of the dense phases, metal, slag and dust phases, are supported by direct measurements through scales and chemical analysis of raw materials and processing co-products. In contrast, the chemistry, volume and flow rates of the produced off-gas phase is computed by the model, because there is not suitable pieces of equipment to provide such data for this study;
- The thermodynamics premises were defined previously regarding the expected minimum content of soluble carbon, silicon and manganese in iron melts, as well the partition coefficient slag-metal of phosphorus. The post combustion ratio at the slag and slag-metal interface is considered

lower than 0.10. On the other hand, post combustion is presumed to occur at the gas phase above the slag, in the range of 0.10-0.80. This range is consistent with other EAF facilities where such on-line measurements are available;

- The off-gas flow rate is not measured, thus, the infiltration air is not included for gas phase calculation. Hence, the oxygen content in surrounding atmospheric air which infiltrates in the EAF control volume is considered non-reactive;
- A number of other factors are also important for the model predictions. Some of them primarily depend on the specific EAF operation, and may vary from furnace to furnace, even from heat to heat. As discussed latter, up to 10-15 kg/t of iron oxide leaves the furnace as dust, mainly coming from the rust and impurities charged within the scrap. Contribution from the bursting effect of ejected metal phase droplets [95] is neglected for dust weight generation, but assumed to be fully incorporated by the slag;
- Moreover, major variables such as the scrap and pig iron melting rates and the post combustion ratios are calculated. The way the scrap is layered in bucket and its apparent density determines the efficiency of its pre-heating, and consequently, its melting rate. For significant amount of charged pig iron, the melting rate will define the available carbon in the melt all over the heat time. Therefore, improper estimate for both melting rates could create uncertainties in the model predictions.
- The GRG (generalized reduced gradient) objective function was defined for minimization of the differences between the model prediction and the experimental results regarding: C and P in the metal phase and for CaO, MgO, SiO₂, FeO in the slag phase composition.